OCEANOGRAPHY

Nanocrystals as phenotypic expression of genotypes—An example in coralline red algae

Gerald Auer[1,2]* and Werner E. Piller[2]

Coralline red algae (CRA) are important ecosystem engineers in the world's oceans. They play key roles as primary food source and carbonate producers in marine habitats. CRA are also vital for modern reef systems where they act as substrate for coral growth and stabilizers of reef frameworks. However, morphotaxonomic identification of these important marine organisms is hampered by the fact that morphological concepts used for their classification do not correspond to molecular data. We present the first analysis of nanoscale features in calcified cell walls of CRA in a globally distributed sample set. We use new morphological traits based on these cell wall ultrastructures to construct an independent morphological phyletic tree that shows a promising congruency with existing CRA molecular phylogenies. Our results highlight cellular ultrastructures as a tool to define the phenotypic expression of genotypic information showing their potential to unify morphology with molecular phylogeny.

INTRODUCTION

Biomineralization, in its strictest sense (1, 2), follows similar basic principles in all organisms. In general, the mineralized skeleton produced by this process is highly ordered (2–5) and forms the basis for a branch of morphotaxonomy, which is applied in modern but, especially, fossil taxonomy. Skeletal mineralization occurs in biologically controlled microenvironments producing mineral precipitation along an organic matrix (1, 2, 6). Specifics of these organic-mineral interactions are still poorly understood, with only recent methodological advancements providing much needed insights (7). Despite these issues, studies of several organism groups have shown that the morphology—but not necessarily the chemistry—of skeletal ultrastructures is strictly biologically controlled and thus not easily perturbed by environmental conditions such as changing pH levels in the ocean (7–12). Consequently, the effect and interplay of environmental and climatological changes on these mineral precipitates are of increasing interest not only in the face of modern climate change but also in the geological past (9, 10, 12, 13).

In microscopic organisms such as foraminifera (5, 14) and coccolithophores (15), the use of these microstructures and ultrastructures has a long and successful history of producing reliable morphotaxonomies that show a high degree of overlap with molecular phylogeny down to the (sub-)species level (3, 5, 14, 15). In particular, the definition of previously unidentified ultrastructural morphologic features in the outer layer (extrados) of miliolid benthic foraminiferal tests provided morphological criteria that are relevant on a generic to suprageneric level and are independent of the ontogenetic development (16).

Yet, despite these historically successful applications, micro- and ultrastructure-based morphotaxonomy is still in its infancy for most macroscopic organism groups. In this context, coral microscale morphology, in particular, has recently received much attention (4, 8, 17, 18). Detailed morphological description of scleractinian corals defined morphologic criteria that are in close congruence with

molecular data (19) and have been tested for several clades [e.g., Mussidae (20), Lobophylliidae (21), and the Merulinidae, Montastraeidae, and Diploastraeidae (22)]. Combined with molecular phylogeny, such studies heralded the revision of scleractinian coral taxonomy on every phylogenetic level (8, 17–20). These recent advances have had a great impact on our understanding of both biogeographic and evolutionary aspects of global scleractinian coral distribution (17, 20, 21, 23, 24).

In this study, we present a new step toward advancing this nascent field of research by applying nanoscale morphotaxonomy to coralline red algae (CRA; orders Corallinales, Hapalidiales, and Sporolithales). We investigate the taxonomic value of nanometer-scale ultrastructures within the calcified CRA thallus by comparing these independent morphologic data to existing molecular phylogenies. This is the first time that the taxonomic potential of skeletal nanometer-scale ultrastructures is tested in macroscopic organisms, which, to date, have only been applied in microscopic algae such as coccolithophores (3) and, to a lesser degree, in diatoms (25). Moreover, biomineralization in CRA represents a unique but still poorly understood feature in nature: Calcification in CRA occurs as the precipitation of high-magnesium calcite along the polysaccharide microfibrils within the organic walls of individual cells (26–29). Understanding taxon-specific differences in CRA ultrastructures may thus provide information that can elucidate the evolutionary implications of biomineralization in CRA (30, 31).

Calcifying red algae are a vital component of modern shallow marine ecosystems (12, 26, 32, 33). In particular, nongeniculate (i.e., fully calcified) (34) CRA act as "bioengineers" modifying ecosystems by creating microhabitats (32) and as essential contributors to the initiation of coral reef development and stabilization of existing reef frameworks (26, 32) or reef builders in the subarctic [e.g., (33)]. As a vital part of almost all tropical to polar shallow marine ecosystems, CRA are important contributors to marine primary productivity and provide a vital food source for benthic grazers (32, 35). The heavily calcified thalli of CRA also make them major carbonate sediment producers. Their carbonate skeletons also lead to an excellent paleontological record of the globally ubiquitous occurrence of CRA at least back to the Mesozoic era (36) and make them promising high-resolution (paleo-)environmental recorders (26, 37, 38). The often-overlooked ecological significance of CRA makes it imperative that

[1]Research Institute for Marine Resources Utilization (Biogeochemistry Program), Japan Agency for Marine-Earth Science and Technology (JAMSTEC), 2-15 Natsushima-cho, Yokosuka, Kanagawa 237-0061, Japan. [2]University of Graz, Institute of Earth Sciences (Geology and Paleontology), NAWI Graz Geocenter, Heinrichstraße 26, 8010 Graz, Austria.
*Corresponding author. Email: gerald.auer@jamstec.go.jp

we better constrain their taxonomy to fully understand the evolutionary adaptation and ecological significance of individual taxa beyond their vast capacity for ecophenotypic growth forms (30–32, 36). While several studies already put increased emphasis on the mineralogy and chemical composition of calcified cell wall ultrastructures of CRA (29, 33, 38), only recently was the organic microfibrillar ultrastructure also considered (28, 29). Despite this growing awareness, the influence of microfibril structures on crystallite shape and (potentially) chemical composition has never been studied in a taxonomic and/or evolutionary context.

RESULTS

Scanning electron microscope (SEM) imaging of the cell walls (Figs. 2 to 4 and figs. S2 to S8) of individual cells within CRA thalli revealed structures matching the four distinct layers fitting the cytological model of plant and algal cells (39–42) (Fig. 2): (i) The plasma membrane, the innermost layer, and the boundary between cytosol and cell organelles serve as the attachment surface for the cell wall; (ii) the primary cell wall (PW) formed during cell growth; (iii) the secondary cell wall (SW) formed on the interior of the primary layer; and (iv) the middle lamella (ML) represents the interface between cells.

Studies dealing with CRA cell wall calcification and the (bio-) chemical composition of microfibrils in the cell walls of CRA and other red algae show that they are composed of cellulose, lignin, and various polysaccharides including not only carrageenans (sulfated polysaccharides) (43) but also chitin (27). Calcification in CRA is also strongly related to their photosynthetic activity and thus cell metabolism (10, 44). Following these base assumptions, our analyses of SEM images confirmed that CRA calcification occurs in two distinct phases within the cell wall, which we herein describe in a (often overlooked) cytological and cell ontogenetic context (Figs. 1 to 4 and see the Supplementary Materials).

Primary calcification

Primary calcification represents the initial calcification step likely associated with sulfated xylogalactans (43), starting immediately after cell division within the PW and the ML (40, 41). Primary calcification forms primary crystallites of high-magnesium calcite (29), which are embedded in the ordered microfibrillar structure of the PW and ML (Figs. 2, 3, and 4.2 and fig. S2) following the preferred arrangement of the cellulose and polysaccharide microfibrils (45). The association of primary crystallites with the cell wall and their orientation are well known in the literature (28, 29, 41, 46), but their growth history has never before been documented in detail: Primary calcification is readily visible on epithallial cells and meristem cells within the coralline algal thallus where the SW is not yet fully developed (Figs. 3, 4.5, and 4.6). Deeper within the thallus, the individual primary crystallites become less obvious and are usually obscured by predominantly granular crystallites associated with ongoing calcification along the PW and ML within the mature thallus (Figs. 3 and 4.4) (44). The initial primary calcification and ongoing calcification of the PW and ML act together to form what is referred to as interfilament calcite (11, 29, 47), the "ML" (46), or interstitial calcite (48), respectively, by various research groups. All of these naming schemes directly refer to the appearance of this layer as a clear visual boundary between CRA cells and, especially, filaments in particular (Figs. 2, 3, and 4.3 and fig. S2.3 to S2.6). It is, however, important to emphasize that these features are not strictly analogs to the ML in a cytological
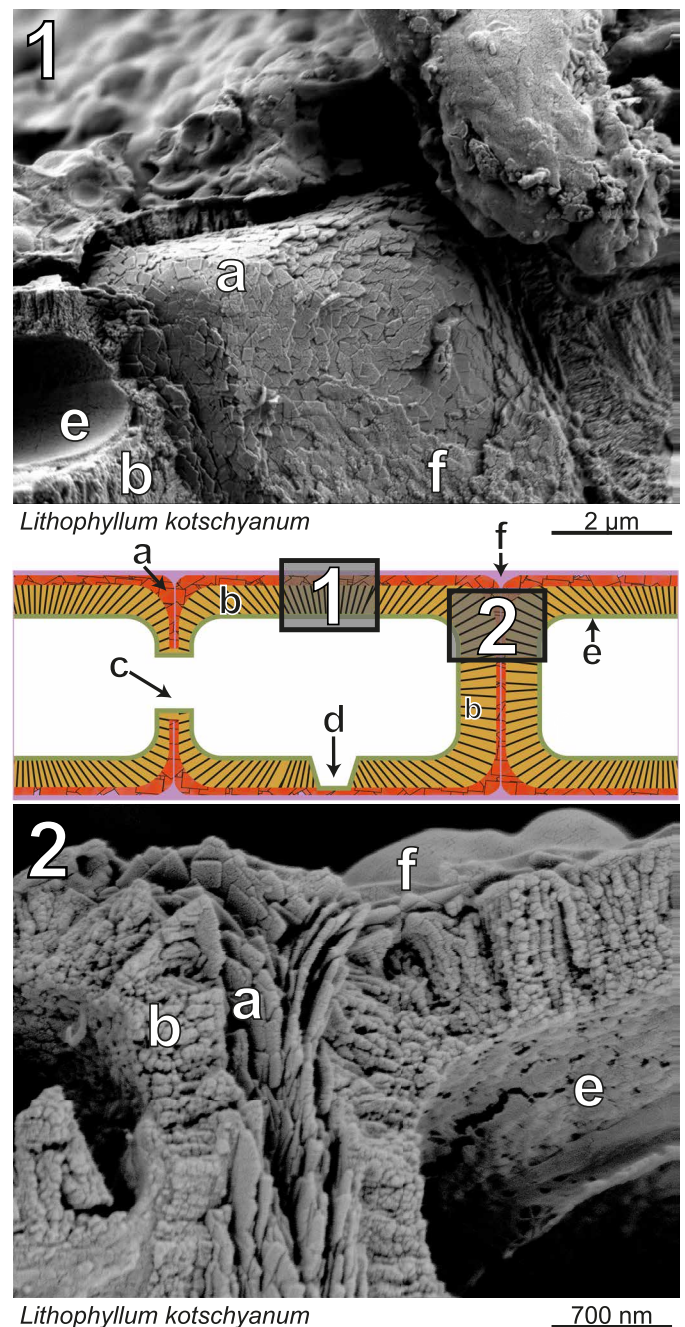

Lithophyllum kotschyanum   2 µm

Lithophyllum kotschyanum   700 nm

Fig. 1. Basic CRA cell wall ultrastructure. SEM images of epithallial cells of *L. kotschyanum* (Sesoko-jima, Japan; see Supplementary Materials for lower-magnification image of the same specimen) and a sketch showing the idealized organization and features of a CRA cell with numbered rectangles representing the position of the SEM images (**1**) and (**2**): (a) rhombohedral PW crystallites of *Lithophyllum* (see Fig. 5); (b) SW crystallites organized in perpendicular rods typical for the *Lithophyllum*-type cell wall (Fig. 2); (c) cell fusions or secondary pit connection connecting two adjacent filaments; (d) primary pit connection connecting the cells within CRA filaments; (e) innermost organic layer (i.e., the plasma membrane; Fig. 2) lining the interior of the calcified SW; and (f) outermost organic cell wall layer equivalent to the surface of the ML (see Fig. 2).
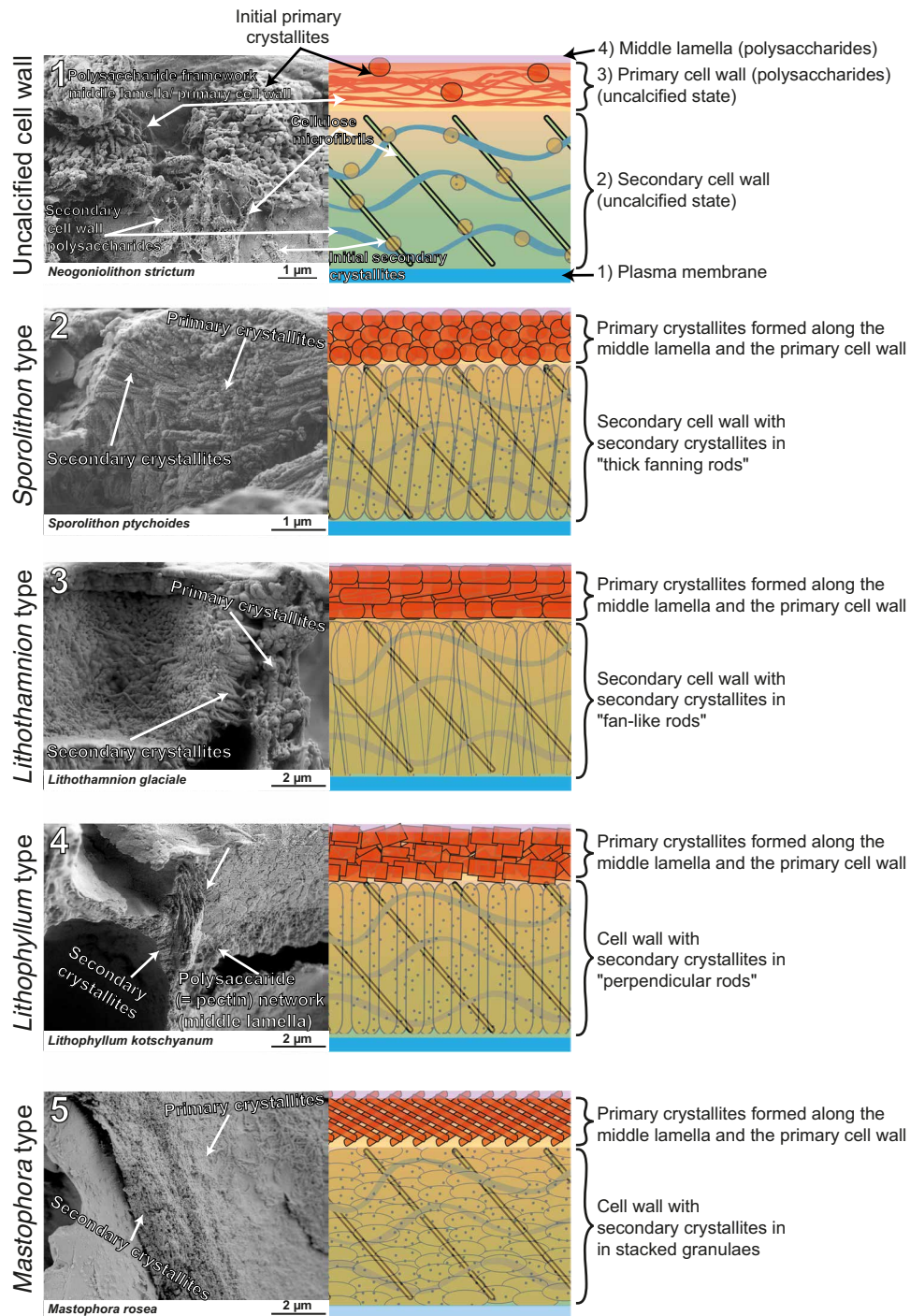
Fig. 2. Cell wall organization and the four CRA cell wall types. (**1**) Crystallites forming along polysaccharide filaments of a recently divided cell with a not yet fully calcified cell wall (*N. strictum*). The model showing the organic components in the CRA cell wall (1) is based on ultrastructure research on both higher plants and algae including CRA (*27*, *40*, *42*, *45*). (**2**) Fanning rod-like crystal aggregates formed by the SW polysaccharide matrix of the Sporolithaceae (*Sporolithon* spp.). (**3**) Dense crystal fans of the *Lithothamnion*-type SW present in the Hapalidiaceae (*L. glaciale* and *Phymatolithon* sp.). (**4**) Perpendicular rod-shaped crystal structures of the *Lithophyllum*-type SW (*Porolithon* spp., *Hydrolithon* sp., *Lithophyllum* spp., and *Titanoderma* sp.). (**5**) *Mastophora*-type cell wall with the SW crystallites organized in undifferentiated layers (*Mastophora* sp.; *Neogoniolithon* spp.).

sense (*42*) and should thus be used with caution (Figs. 2 and 3). We consequently retain the use of the classical term "primary layer" (*41*) for calcite precipitated within the PW and ML to avoid confusion with the term ML as used in cytology.

Secondary calcification

Secondary calcification occurs within the SW (*6*, *41*) and is generally produced by cells within the mature thallus (Figs. 2 to 4 and Supplementary Materials), although it is also rarely observed in epithallial
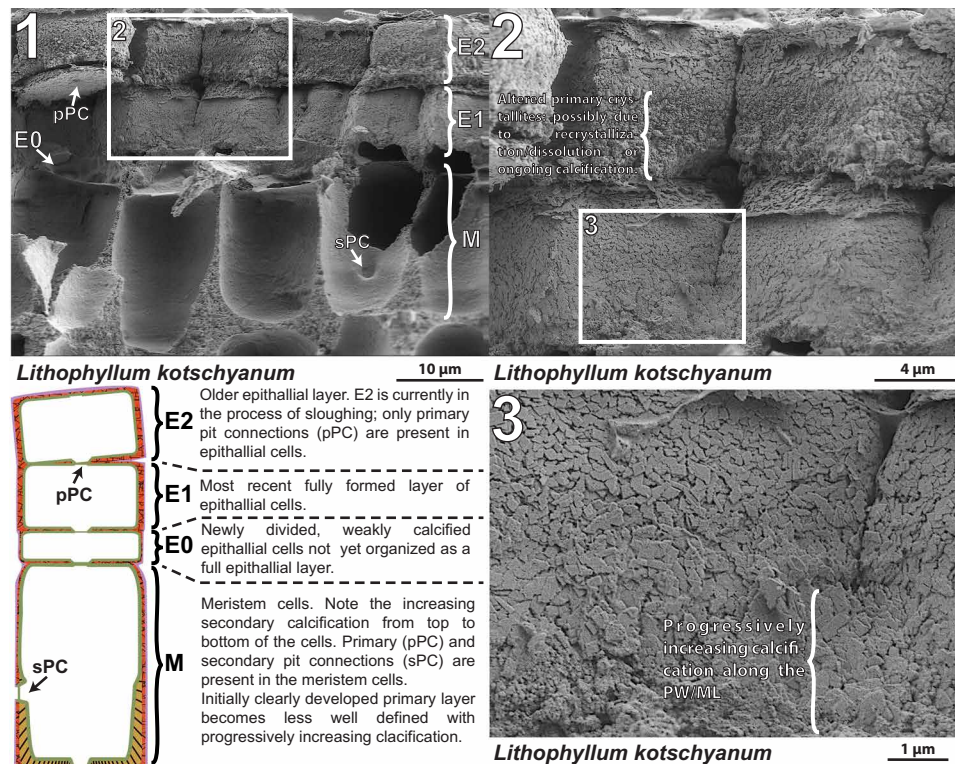
Fig. 3. Detail of the generalized CRA thallus structure. (**1**) Overview and graphical representation of the *L. kotschyanum* (Guam) thallus showing two fully formed epithallial layers and several recently divided epithallial cells above meristem cells that show increasing secondary calcification toward their lower base. (**2**) Enlarged SEM image showing the two epithallial layers; the lower portion of the cells with alteration of the primary crystallites at the contact surface between cells of E2. This effect is likely related to ongoing calcification in the PW and the ML between cells, although dissolution due to seawater interactions cannot be fully disregarded for the alteration present in E2. (**3**) Further close-up of E1 showing clear ongoing calcification along the PW and ML merging individual crystallites leading to their typical appearance seen in the primary layer (= interfilament calcite).

cells (Fig. 1 and fig. S1). The orientation of the calcite crystallites within the SW follows the orientation of the layered polysaccharide matrix and the columnar structural cellulose (Fig. 2) (*29*, *41*).

SW calcification produces the bulk of the calcite found in the CRA thallus and continues to form throughout the life span of the cell (*44*). Secondary calcification occurs inward toward the center of the cell, thickening the cell wall while reducing the cell space itself (Figs. 2 and 4.5 and fig. S1) (*10*, *40*).

Comparative morphotaxonomy

Our comparative analysis of the SW types showed a clear congruence with the major groups of CRA established by classical morphology (based on the presence of uniporate and multiporate conceptacles or sori) and molecular phylogeny (Figs. 2 and 5). Comparison of the cell wall structures of CRA with uniporate conceptacles (i.e., belonging to the family Corallinaceae), however, showed two distinct SW organization types (Fig. 2; see figs. S7 and S8 for detailed images). Notably, the *Mastophora*- and *Lithophyllum*-type SW are synonymous with the *Goniolithon*- and *Lithophyllum*-type calcification described by Flajs in 1977 (*41*). In summary, the epithallial and meristem cells of all available CRA taxa further showed that crystallites formed by primary and secondary calcification are highly ordered and structurally distinct (Figs. 2, 4, and 5; see the Supplementary Materials). Following morphological comparisons of the data, we define eight distinct morphotypes of primary crystallites, which appear strongly

differentiated between individual subfamilial clades as defined by molecular phylogeny (Fig. 5 and fig. S9) (*49*). To test the validity of these new morphological criteria, we applied parsimony analysis using PAUP* [Phylogenetic Analysis Using Parsimony (*and Other Methods)] (*50*). The results of the PAUP* analysis are based on a binary matrix that includes all characters classically defined in the calcified CRA thallus (*34*) augmented by newly defined morphological characters derived from the identified cell wall ultrastructures. Results of the PAUP* parsimony analysis strongly support our hypothesis that the established ultrastructure-based characters are taxonomically viable and that the genotype of CRA is expressed within the nanoscale ultrastructure of the PW and SW crystallites (Figs. 2 to 4 and 5; see Supplementary Materials).

DISCUSSION
The issues with classical CRA morphotaxonomy

Until now, CRA morphotaxonomy was based on the growth forms of the CRA thallus, as well as the organization of specific soft tissue structures within their specialized reproductive organs, called sori or conceptacles (*34*). As the morphology of the CRA thallus can be highly diverse even for the same species (*31*, *32*, *34*), traditional morphological approaches are often of little use. The resulting incongruities between molecular and morphologic data consequently lead to the conclusion that classical, morphology-based phylogeny
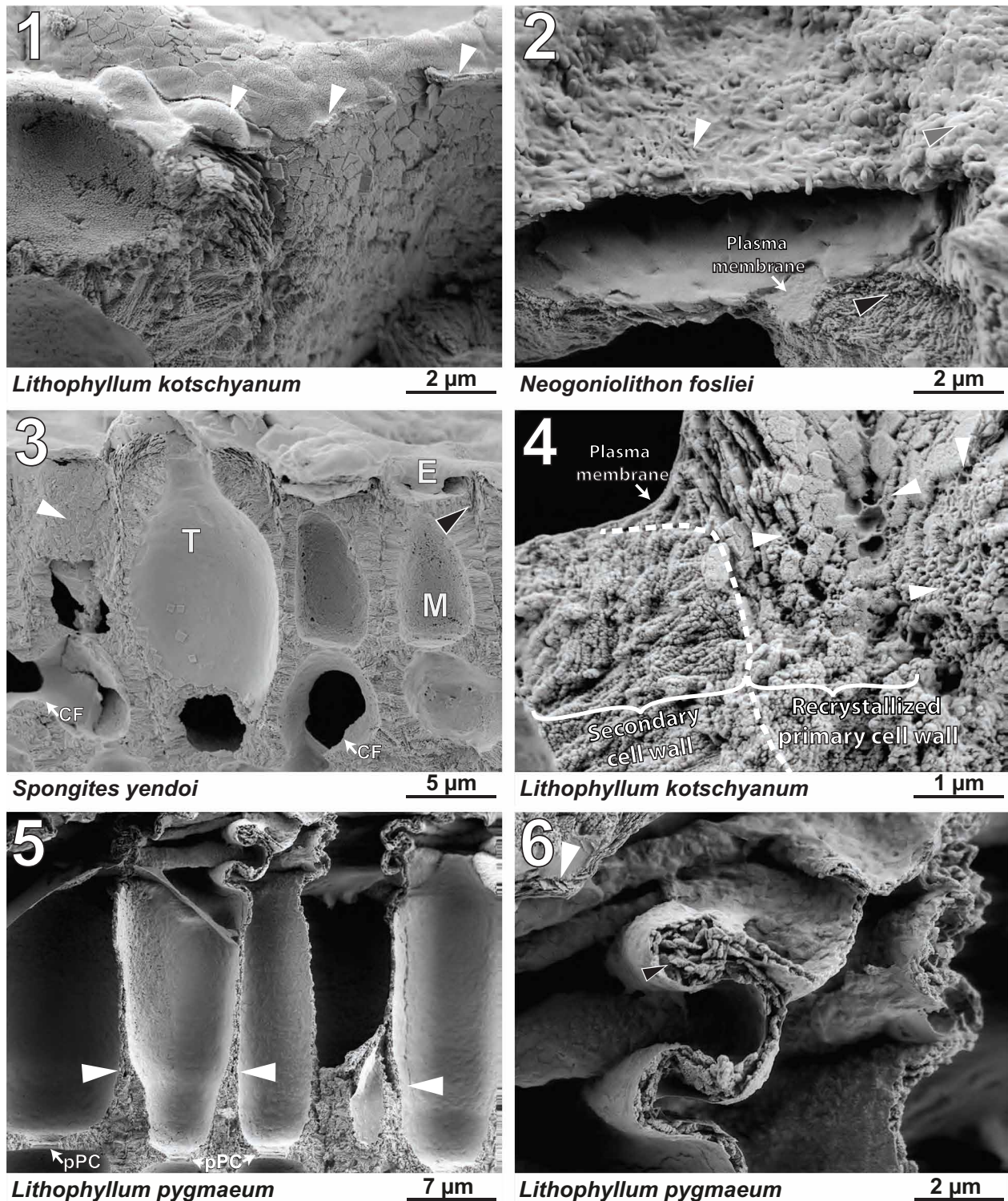
Fig. 4. PW calcification. (**1**) PW crystallites covering epithallial cells of *L. kotschyanum* (Dubai). White arrowheads indicate the organic layer covering the crystallites. (**2**) Epithallial cell of *N. fosliei* (Safaga, Egypt) covered by rod-shaped crystallites (white arrowhead) within an organic matrix (gray arrowhead). Interior of the cell wall consists of primary crystallites (black arrowhead) surrounding the inner cell wall (= plasma membrane). (**3**) Recrystallization of primary crystallites along an exposed PW of *S. yendoi* (Japan; white arrow). Black arrowhead points to primary crystallites fusing into the PW (= ML) between the epithallial (E) and meristem cells (M); note the thickened cell wall of the trichocyte (T) and cell fusions (CF). (**4**) Close-up of an epithallial cell wall and fully calcified meristem cell. The dashed line separates the secondary and recrystallized PW. White arrowheads show polysaccharide microfibrils. (**5**) Meristem of *L. pygmaeum* (Guam) showing cell elongation during enhanced thallus growth. White arrows show SW terminations. Cell wall calcification above is very weak, which led to cells becoming squashed during specimen preparation (seen also in Fig. 3). (**6**) Close-up of the squashed part (5), with primary crystallites in the PW (white arrowheads). pPC, primary pit connection.
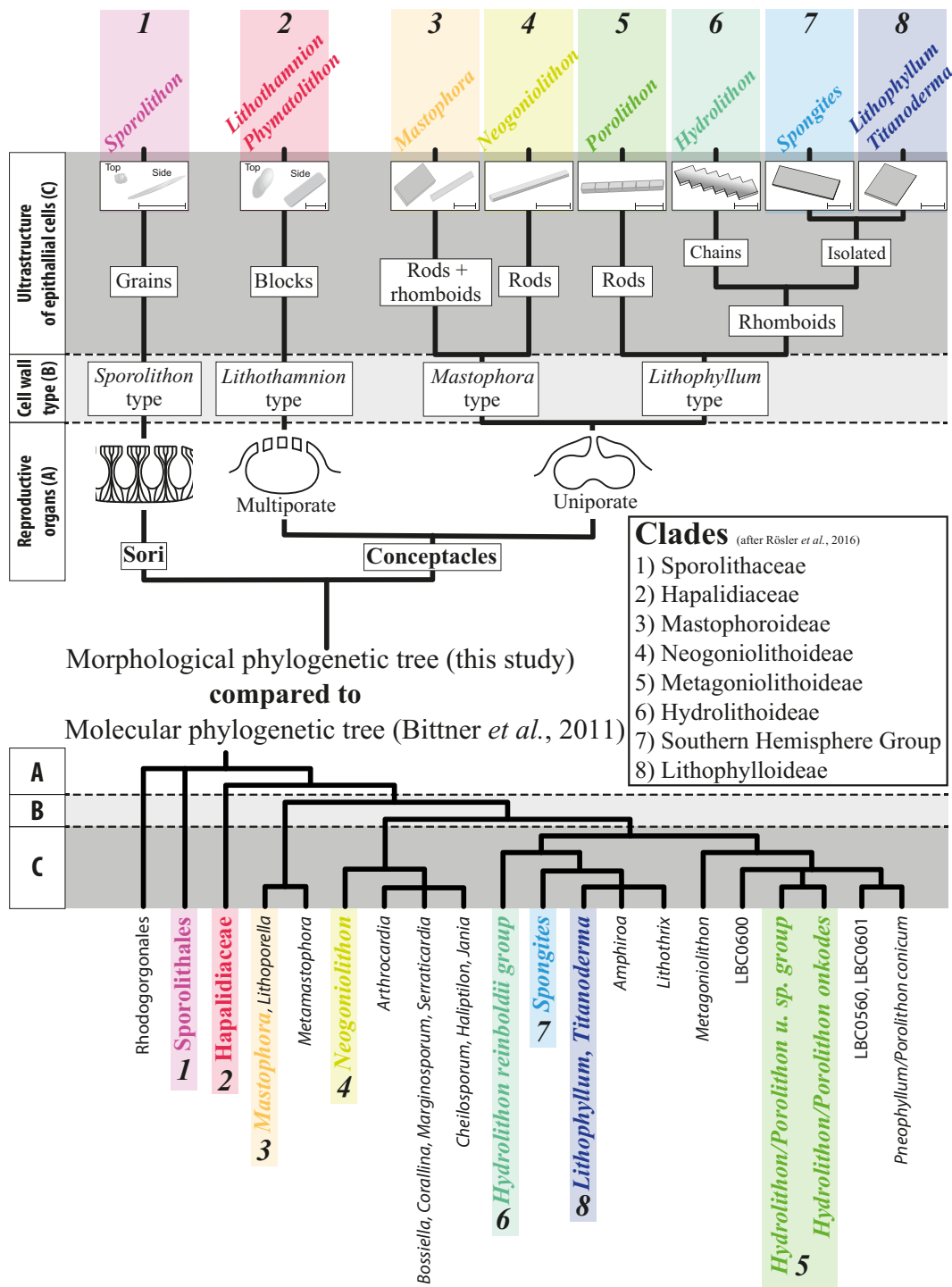
Fig. 5. Comparison of molecular and morphologic phylogeny. Upper phylogenetic tree shows the hierarchical position of the major diagnostic morphological characters used herein. The proposed tree is compared to the ribosomal loci (SSU and LSU) and encoding markers (psbA and COI) derived from the molecular phylogeny of Bittner *et al.* in 2011 (*51*) and allows the identification of all major molecular phylogenetic clades of Corallinacea [sensu Rösler *et al.* (*49*)] and distinguishing them from the Sporolithaceae and Hapalidiaceae based on three easily identifiable morphological features: (**A**) reproductive organs, (**B**) SW structures (see Fig. 2), and (**C**) the dominant morphotype of epithallial cell wall crystallites. (1) *Sporolithon*: granules; (2) Hapalidiaceae (*Lithothamnion* and *Phymatolithon*): blocks and granules; (3) Mastophoroideae (*Mastophora* sp.): rods and rhombic plates; (4) Neogoniolithideae (*Neogoniolithon* spp.): (hexagonal) rods; (5) Metagoniolithoideae (*Porolithon* spp.): rhombic blocks organized in rods; (6) Hydrolithoideae (*Hydrolithon* sp.): rhomboids organized in chains; (7) SHG (*S. yendoi*): elongated rhombic plates; (8) Lithophylloideae (*Lithophyllum* spp./*Titanoderma* sp.): rhombic plates (sometimes irregularly fused). Detailed SEM images of the diagnostic cell wall ultrastructures can be found in Supplementary Materials. The DNA sequence–based phylogenetic clades and names assigned to these clades were adapted from Bittner *et al.* (*51*) and not updated to more recent DNA sequence–based revisions of CRA phylogeny (*49*).

does not coincide with molecular data (*51*). In particular, the molecular phylogenetic studies by Bittner *et al.* (*51*), Kato *et al.* (*52*), and, more recently, Rösler *et al.* (*49*) highlighted the need for a revised morphological taxonomy (see the Supplementary Materials for details). Our results indicate that the taxonomic incongruities between molecular phylogeny and CRA morphotaxonomy can potentially be resolved by augmenting classical morphological characters with skeletal ultrastructures. These new morphological criteria rely on the highly variable morphology of crystallites formed in the PW layer present on epithallial and meristem cells (Fig. 3; see Supplementary Materials). A key advantage of this new approach is that the defining morphological features are ubiquitous within the CRA thallus and readily observable with high-resolution SEM equipment.

Linking morphology with molecular phylogeny

The described skeletal ultrastructures provide an independent morphotaxonomic concept that appears widely consistent with molecular phylogenic clades/subfamilies (Figs. 2 and 5; see the Supplementary Materials) (*49*, *51*, *52*). Assignment of the *Lithophyllum*-type and *Mastophora*-type SW improves previous morphotaxonomic concepts by grouping *Hydrolithon*, *Porolithon*, and *Spongites yendoi* [Southern Hemisphere group/SHG sensu Rösler *et al.* (*49*)] more closely with *Lithophyllum* than with *Neogoniolithon* and *Mastophora*. This clear separation of the Mastophoroideae and Neogoniolithideae from the clade containing the Metagoniolithoideae, Hydrolithoideae, Lithphylloideae, and the SHG was only previously accomplished by using only rarely present soft tissue features in CRA reproductive organs (*49*). The results of our morphological comparison are thus in accordance with molecular phylogeny (*49*, *51*, *52*) and show that the crystal shapes formed by the secondary calcification step of CRA cells potentially reflect larger phylogenetic groups (Figs. 2 and 5).

On a higher taxonomic level, our independent morphological analysis of nanoscale PW ultrastructures shows a clear correspondence with the phylogenetic clades/subfamilies defined by Rösler *et al.* (*49*) (Fig. 5). In detail, our morphologic approach matches the phyletic position of *Mastophora* and *Neogoniolithon* based on the analysis of "DNA sequences of small subunit (SSU) rDNA and plastid-encoded gene of PSII reaction center protein D1 (psbA)" sensu Kato *et al.* (*52*), while our placement of *S. yendoi* (SHG), *Porolithon* spp. (Metagoniolithoideae), Hydrolithoideae, and the Lithphylloideae matches with the "small and large ribosomal subunit loci (SSU, LSU), psbA, and mitochondrial gene encoding cytochrome c oxidase subunit I (COI)" approach used in dataset 2 of Bittner *et al.* (*51*). Our results do not match the cladograms obtained from only using SSU DNA sequences [dataset 1 of Bittner *et al.* (*51*)] and the five DNA marker approach (SSU, LSU, psbA, COI, and 23S) of Rösler *et al.* (*49*), which place the Hydrolithoideae into a greater distance from the Lithophylloideae than the Metagoniolithoideae. Thus, our data match best with the results of molecular phylogenies based on ribosomal loci (SSU and LSU) and encoding markers (psbA and COI) (*51*), with only the position of Mastophoroideae and Neogoniolithoideae not in full agreement.

In conclusion, it seems that the exact molecular phylogenetic placement of these CRA subfamilies remains heavily dependent on the specific gene marker approach used. This is likely a result of the inherent natural variability that limits the usefulness of individual gene sequences for phylogenetic studies. In general, however, our morphological data match key aspects of all investigated molecular phylogenetic trees, providing evidence that these ultrastructural features are valuable descriptive features at least on the subfamilial level. Analysis of these ultrastructures may also help to resolve uncertainties between molecular phylogenies derived from various gene sequences: Our study provides independent morphotaxonomic evidence for the close relationship for the SHG with the Lithophylloideae. We also confirm the monophyly of *Hydrolithon* within the Hydrolithoideae while separating this taxon from *Porolithon* spp. (Fig. 5) as formalized by Kato *et al.* (*52*) and evident in all other considered molecular phylogenies (*49*, *51*, *53*).

Because of a lack of available specimens in the order Hapalidiales, we were unable to separate this clade further in this study. However, Adey *et al.* (*33*) published molecular data for several Hapalidiales taxa and defined an intricate array of congruent morphological criteria, albeit without considering ultrastructures. Analysis of these specimens would thus be ideal to test our independent ultrastructure-based taxonomic criteria in the order Hapalidiales. Furthermore, several previous studies provide high-resolution images of several Hapalidiales genera including not only *Phymatolithon* (*29*) but also *Clathromorphum*, *Lithothamnion*, *Leptophytum* (*28*, *33*, *38*, *46*), and *Kvaleya* (*28*). The presented image material in these studies provides strong support for the consistency of our proposed morphological features with the phylogenetic clades proposed by Rösler *et al.* (*49*), by showing structurally different primary crystallites present in the "interfilament calcite" (= primary calcification) described in these studies.

Evolutionary and ecological implications of CRA ultrastructures

From an evolutionary standpoint, there seems to be a clear increase in ultrastructure complexity from sori bearing *Sporolithon* to the uniporate conceptacle bearing Corallinaceae, with the multiporate Hapalidiaceae occupying an intermediate position. The reduction in complexity of the SW of the Neogoniolithidae and the Mastophorideae may represent a (syn-)apomorphic trait that developed after their divergence from other clades in the Corallinaceae. We further hypothesize that the observed morphologic diversity of ultrastructure is based on the fact that nanoscale biomineralization in CRA occurs only along these organic templates. The direct association with such organic templates limited to a specific cell structure is broadly comparable to the calcification along the base plates in coccolithophore cells (*3*).

Our findings directly highlight the strong biological control of calcification along fixed organic templates in CRA, confirming that it is biomineralization in a strict sense. The morphological difference between the PW and SW crystallites highlights the radically different organization of the organic matrix present in the PW and SW. Further evidence that primary calcification and secondary calcification are controlled by distinct metabolic processes/pathways is offered by the fact that the magnesium-to-calcium ratio of PW and SW calcite is also radically different (*28*). In light of these findings, we see an increasing need to analyze the mineralogy and chemical composition of taxon-specific nanoscale ultrastructures to fully characterize their calcification pathways and make definitive statements on their formation mechanism in the context of phylogenetic data.

We also note that primary calcification of epithallial cells may occur relatively fast and may represent a notable ecological advantage. Besides a potential benefit to photosynthesis by regulating pH and CO_2 concentrations within the cell (*54*, *55*), fast calcification of epithallial cells may benefit CRA as a protective layer against not only desiccation (especially in intertidal habitats) but also grazing

and/or ultraviolet light. As there is now good evidence that different taxa develop different primary ultrastructures, it will also be interesting to explore why some taxa develop several micrometer-thick thickly calcified cell walls (see fig. S2.1 and 2.4), while others generally do not (Fig. 3). This avenue of research becomes important to understand the difference of evolutionary versus ecophenotypical adaptation of CRA to their preferred habitat and/or herbivore pressure and the development of sloughing as an antifouling mechanism (30, 35, 36, 56).

Furthermore, we also present evidence that PW and SW formation and calcification are intrinsically linked with cell growth: Portions of the thallus that exhibit strong cell elongation do not exhibit well-defined secondary calcification. This confirms that SW calcification only occurs after the cell has fully matured, similar to SW growth in higher plants (39). Evidence that meristem cells form only primary crystallites during elongations further highlights the strong interplay of cell growth and calcification (Figs. 3, 4.5, and 4.6).

Outlook and implications for nanoscale morphotaxonomy
Here, we provide first evidence for the expression of genotypic information in CRA skeletal ultrastructures and postulate that calcification along the microfibrillar matrix of CRA cell walls has a high propensity for taxon-specific crystallite morphology. Despite this notable advance toward a unification of morphological and molecular phylogenetics in CRA, our results only represent a first step. Further research in close conjunction with molecular phylogenetic analysis will be necessary to expand upon these findings, with important next steps being (i) the documentation of cell wall ultrastructures in the Hapalidiaceae, the largest order of CRA, and (ii) an in-depth comparative analysis that focuses on multiple taxa in single clades/subfamilies to document interclade morphological variability.

This study shows the potential of micro- and/or nanoscale phenotypic characters to bridge the fields of organismal biology and molecular biology. Linking these two disciplines will be crucial to our understanding of how evolutionary changes in genetic code interrelate with the adaptation of organisms to their environment. Our approach consequently provides a way forward to resolve taxonomic questions for organism groups, where classical morphological approaches fail to fully reflect genotypic variation. By improving morphotaxonomic concepts used in both modern taxonomy and the fossil record, it becomes possible to unify the paleontological record with modern molecular phylogeny similar to the advances made in sea urchins (57), foraminifera (14, 16), and scleractinian corals (24). Ultimately, such ultrastructural approaches can also provide independent information/verification where gene plasticity results in conflicting molecular phylogenies (see above for an example on CRA).

This study ultimately highlights the need and potential of detailed and integrative studies of skeletal ultrastructure-based approaches to complement molecular phylogeny. Only the integration of both recent and fossil morphological with molecular data will provide accurate information on the evolutionary relationships of taxa, not only in CRA but also in many other organism groups.

MATERIALS AND METHODS
CRA was selected as a term to refer to calcifying red algae in this work, with the intention of using a taxonomically neutral term. The term CRA can thus include all red algae that calcify, including all growth forms of both crustose and articulate (geniculate) calcareous red algae, although only nongeniculate algae exhibiting calcitic biomineralization were analyzed during this study.

Samples were obtained from a combination of several sampling campaigns, existing collection material at the Institute of Earth Sciences at the University of Graz (56, 58), and donations of private and international scientific collections. For SEM analysis, ≥3 fracture samples were prepared for each specimen in all sampling sites (see table S1 for the number of specimens analyzed from each taxon at a specific sample locality).

Specimens were washed, air-dried, and carefully cleaned from epiphytes. Small tongs were used to break off several branches from larger CRA rhodoliths, while crusts were carefully separated from their substrate using a medical scalpel and split into pieces. The fractured pieces of CRA crusts and rhodolith branches were then split with a medical scalpel and/or small cutting tongs when necessary. Between 5 and 10 pieces per specimen were oriented in the direction of growth and mounted on SEM stubs using conductive graphite tape and grounded using colloidal silver. Stub-mounted samples were sputtered with Au/Pd using an Edwards Scancoat Six sputter coater and then analyzed in a Zeiss Gemini DSM 982 field emission SEM under high vacuum conditions. SEM imaging was performed at the Institute of Earth Sciences at the NAWI Graz Geocenter, University of Graz. Several different settings were tested for the SEM analyses, with low acceleration voltages (2 kV) and low working distances (5 mm) yielding the best results. Higher acceleration voltages (≥10 kV) proved to be unsuitable, since the penetration depth of the SEM electron beam became too high, obscuring the delicate features of individual crystallites. This effect was particularly apparent during the study of epithallial cells, since high acceleration voltages completely obscured the thin (~500 nm to 1 μm) calcification of these cells. High penetration depths lead to a fuzzy and/or "translucent" look of the image that obscures most taxonomically relevant features. Combining signals from an external and an in-lens secondary electron (SE) detector also improved the imaging quality. Mixing the two SE detectors visibly improved the resolution of individual nanometer-sized crystallites on the epithallial cells. In general, however, using a single (preferentially external) SE detector is suitable to successfully identify even the smallest primary crystallites encountered in this study.

Before ultrastructural analyses, all samples were identified at the genus level, and at the species level if possible, using classical taxonomic characters proposed by Woelkerling (34). This approach was chosen on the basis of the fact that CRA species are classically described based on morphological features and not molecular phylogeny. We thus use an independent morphological framework (see the Supplementary Materials for details), which was then compared to established molecular phylogenies (49, 51, 52). For this reason, we also elected to keep the morphotaxonomical species names intact for many samples to more easily distinguish between different morphotypes within our identified genera. To allow accurate comparison of all considered taxa with molecular phylogenies, only specimens that could be reliably identified and assigned to genera that have reliable position within molecular phylogenies were further considered for this analysis. We also preferentially selected taxa that were recovered at multiple sample locations to avoid biases in our analysis based on changing environmental conditions. We chose this approach to ensure reliable results without the need of molecular phylogenetic methods, although this limited taxon diversity in most considered clades (particularly the SHG and the Hapalidiaceae). Key morphological

features were collected in a matrix and used to generate a phylogenetic tree with PAUP* version 4.0 (*50*). The used matrix of morphological criteria includes all classically used characters (*34*) as well as the ultrastructures defined within this study, resulting in 19 morphological criteria with their presence/absence noted in all 15 taxa (table S2). The criteria are listed as a binary matrix with 1 = presence and 0 = absence in each taxon. This presence/absence matrix approach is consistent with classical CRA morphotaxonomy but extends classically used criteria in the CRA thallus (*34*) with newly defined traits.

SUPPLEMENTARY MATERIALS

Supplementary material for this article is available at http://advances.sciencemag.org/cgi/content/full/6/7/eaay2126/DC1

Fig. S1. Supporting image to Fig. 1, showing the heavily calcified thallus portion of this specimen of *Lithophyllum kotschyanum* (Sesoko-jima, Japan).

Fig. S2. Primary and secondary crystallization of *Porolithon gardineri* (Safaga, Egypt).

Fig. S3. Morphological overviews of *L. kotschyanum* (Safaga, Egypt), *Lithophyllum pygmaeum* (Dubai, United Arab Emirates), *Titanoderma byssoides* (Gavdos, Greece), and *S. yendoi* (Sesoko-jima, Japan).

Fig. S4. Morphological overviews of *Porolithon okodes* (Safaga, Egypt), *P. gardineri* (Safaga, Egypt), and *Hydrolithon reinboldii* (Hawaii, USA).

Fig. S5. Morphological overviews of *Neogoniolithon strictum* (Florida, USA), *Neogoniolithon fosliei* (Safaga, Egypt), and *Mastophora rosea* (Guam).

Fig. S6. Morphological overviews of *Lithothamnion glaciale* (Rebbenesøya, Norway) and *Phymatolithon* sp.

Fig. S7. Plate showing the SW structure and exposed primary layers deeper in the coralline algal thallus of *L. kotschyanum* (Safaga, Egypt), *L. pygmaeum* (Guam), *T. byssoides* (Gavdos, Greece), *Porolithon onkodes* (Safaga, Egypt), *Porolithon gardineri* (Safaga, Egypt), *H. reinboldii* (Dubai, United Arab Emirates), and *S. yendoi* (Sesoko-jima, Japan).

Fig. S8. Plate showing the SW structure and exposed primary layers deeper in the coralline algal thallus of *L. glaciale* (Rebbenesøya, Norway), *Phymatolithon* sp. (Rebbenesøya, Norway), *Sporolithon ptychoides* (Safaga, Egypt), *N. strictum* (Rodriguez Key, Florida, USA), *N. fosliei* (Safaga, Egypt), and *M. rosea* (Guam).

Fig. S9. SEM image showing details of the PW crystallites present on the topmost epithallial cell row of the major CRA clades as shown in Fig. 5.

Table S1. List of the analyzed samples with the corresponding locations where the specimens were collected.

Table S2. Binary matrix of morphological criteria assigned for each taxon.

References (*59*–*61*)

View/request a protocol for this paper from *Bio-protocol*.

REFERENCES AND NOTES

1. L. Addadi, S. Weiner, Biomineralization: Mineral formation by organisms. *Phys. Scr.* **89**, 098003 (2014).
2. S. Weiner, P. M. Dove, An overview of biomineralization processes and the problem of the vital effect. *Rev. Mineral. Geochem.* **54**, 1–29 (2003).
3. J. R. Young, S. A. Davis, P. R. Bown, S. Mann, Coccolith ultrastructure and biomineralisation. *J. Struct. Biol.* **126**, 195–215 (1999).
4. J.-P. Cuif, G. Lecointre, C. Perrin, A. Tillier, S. Tillier, Patterns of septal biomineralization in Scleractinia compared with their 28S rRNA phylogeny: A dual approach for a new taxonomic framework. *Zool. Scripta.* **32**, 459–473 (2003).
5. B. W. Hayward, M. Holzmann, H. R. Grenfell, J. Pawlowski, C. M. Triggs, Morphological distinction of molecular types in *Ammonia*—Towards a taxonomic revision of the world's most commonly misidentified foraminifera. *Mar. Micropaleontol.* **50**, 237–271 (2004).
6. M. A. Borowitzka, A. W. D. Larkum, Calcification in algae: Mechanisms and the role of metabolism. *Crit. Rev. Plant Sci.* **6**, 1–45 (1987).
7. O. Branson, E. A. Bonnin, D. E. Perea, H. J. Spero, Z. Zhu, M. Winters, B. Hönisch, A. D. Russell, J. S. Fehrenbacher, A. C. Gagnon, Nanometer-scale chemistry of a calcite biomineralization template: Implications for skeletal composition and nucleation. *Proc. Natl. Acad. Sci. U.S.A.* **113**, 12934–12939 (2016).
8. M. V. Kitahara, H. Fukami, F. Benzoni, D. Huang, in *The Cnidaria, Past, Present and Future* (Springer, 2016), vol. 7, pp. 41–59.
9. L. Beaufort, I. Probert, T. de Garidel-Thoron, E. M. Bendif, D. Ruiz-Pino, N. Metzl, C. Goyet, N. Buchet, P. Coupel, M. Grelaud, B. Rost, R. E. M. Rickaby, C. de Vargas, Sensitivity of coccolithophores to carbonate chemistry and ocean acidification. *Nature* **476**, 80–83 (2011).
10. L. C. Hofmann, M. Koch, D. de Beer, Biotic control of surface pH and evidence of light-induced H$^+$ pumping and Ca^{2+}-H$^+$ exchange in a tropical crustose coralline alga. *PLOS ONE* **11**, e0159057 (2016).
11. M. C. Nash, B. N. Opdyke, U. Troitzsch, B. D. Russell, W. H. Adey, A. Kato, G. Diaz-Pulido, C. Brent, M. Gardner, J. Prichard, D. I. Kline, Dolomite-rich coralline algae in reefs resist dissolution in acidified conditions. *Nat. Clim. Chang.* **3**, 268–272 (2013).
12. M. C. Nash, S. Uthicke, A. P. Negri, N. E. Cantin, Ocean acidification does not affect magnesium composition or dolomite formation in living crustose coralline algae, *Porolithon onkodes* in an experimental system. *Biogeosciences* **12**, 5247–5260 (2015).
13. S. M. Stanley, Influence of seawater chemistry on biomineralization throughout phanerozoic time: Paleontological and experimental evidence. *Palaeogeogr. Palaeoclimatol. Palaeoecol.* **232**, 214–236 (2006).
14. J. Pawlowski, M. Holzmann, J. Tyszka, New supraordinal classification of Foraminifera: Molecules meet morphology. *Mar. Micropaleontol.* **100**, 1–10 (2013).
15. A. G. Sáez, I. Probert, M. Geisen, P. Quinn, J. R. Young, L. K. Medlin, Pseudo-cryptic speciation in coccolithophores. *Proc. Natl. Acad. Sci. U.S.A.* **100**, 7163–7168 (2003).
16. J. H. Parker, Ultrastructure of the test wall in modern porcelaneous foraminifera: Implications for the classification of the Miliolida. *J. Foramin. Res.* **47**, 136–174 (2017).
17. A. F. Budd, J. Stolarski, Searching for new morphological characters in the systematics of scleractinian reef corals: Comparison of septal teeth and granules between Atlantic and Pacific Mussidae. *Acta Zool.* **90**, 142–165 (2009).
18. A. F. Budd, S. L. Romano, N. D. Smith, M. S. Barbeitos, Rethinking the phylogeny of scleractinian corals: A review of morphological and molecular data. *Integr. Comp. Biol.* **50**, 411–427 (2010).
19. J. Stolarski, Three-dimensional micro-and nanostructural characteristics of the scleractinian coral skeleton: A biocalcification proxy. *Acta Palaeontol. Pol.* **48**, 497–530 (2003).
20. A. F. Budd, H. Fukami, N. D. Smith, N. Knowlton, Taxonomic classification of the reef coral family Mussidae (Cnidaria: Anthozoa: Scleractinia). *Zool. J. Linn. Soc.* **166**, 465–529 (2012).
21. D. Huang, R. Arrigoni, F. Benzoni, H. Fukami, N. Knowlton, N. D. Smith, J. Stolarski, L. M. Chou, A. F. Budd, Taxonomic classification of the reef coral family Lobophylliidae (Cnidaria: Anthozoa: Scleractinia). *Zool. J. Linn. Soc.* **178**, 436–481 (2016).
22. D. Huang, F. Benzoni, H. Fukami, N. Knowlton, N. D. Smith, A. F. Budd, Taxonomic classification of the reef coral families Merulinidae, Montastraeidae, and Diploastraeidae (Cnidaria: Anthozoa: Scleractinia). *Zool. J. Linn. Soc.* **171**, 277–355 (2014).
23. A. F. Budd, J. M. Pandolfi, Evolutionary novelty is concentrated at the edge of coral species distributions. *Science* **328**, 1558–1561 (2010).
24. H. Fukami, A. F. Budd, G. Paulay, A. Solé-Cava, C. A. Chen, K. Iwao, N. Knowlton, Conventional taxonomy obscures deep divergence between Pacific and Atlantic corals. *Nature* **427**, 832–835 (2004).
25. A. Witkowski, T. Płociński, J. Grzonka, I. Zgłobicka, I. Zgłobicka, M. Bąk, P. Dąbek, A. I. Gomes, K. J. Kurzydłowski, K. J. Kurzydłowski, in *Diatoms: Fundamentals and Applications*, J. Seckbach, R. Gordon, Eds. (Wiley, 2019); https://onlinelibrary.wiley.com/doi/pdf/10.1002/9781119370741.ch6.
26. D. Basso, Carbonate production by calcareous red algae and global change. *Geodiversitas* **34**, 13–33 (2012).
27. M. A. Rahman, J. Halfar, First evidence of chitin in calcified coralline algae: New insights into the calcification process of *Clathromorphum compactum*. *Sci. Rep.* **4**, 6162 (2014).
28. M. C. Nash, W. Adey, Anatomical structure overrides temperature controls on magnesium uptake—Calcification in the Arctic/subarctic coralline algae *Leptophytum laeve* and *Kvaleya epilaeve* (Rhodophyta; Corallinales). *Biogeosciences* **15**, 781–795 (2018).
29. M. C. Nash, W. Adey, Multiple phases of Mg-calcite in crustose coralline algae suggest caution for temperature proxy and ocean acidification assessment: Lessons from the ultrastructure and biomineralisation in *Phymatolithon* (Rhodophyta, Corallinales). *J. Phycol.* **53**, 970–984 (2017).
30. R. S. Steneck, S. D. Hacker, M. N. Dethier, Mechanisms of competitive dominance between crustose coralline algae: An herbivore-mediated competitive reversal. *Ecology* **72**, 938–950 (1991).
31. R. S. Steneck, The ecology of coralline algal crusts: Convergent patterns and adaptive strategies. *Annu. Rev. Ecol. Syst.* **17**, 273–303 (1986).
32. M. S. Foster, Rhodoliths: Between rocks and soft places. *J. Phycol.* **37**, 659–667 (2001).
33. W. H. Adey, J. J. Hernández-Kantún, G. Johnson, P. W. Gabrielson, DNA sequencing, anatomy, and calcification patterns support a monophyletic, subarctic, carbonate reef-forming *Clathromorphum* (Hapalidiaceae, Corallinales, Rhodophyta). *J. Phycol.* **51**, 189–203 (2015).
34. W. J. Woelkerling, *The Coralline Red Algae: An Analysis of the Genera and Subfamilies of Non-Geniculate Corallinaceae* (Oxford University Press, 1988).
35. D. W. Keats, M. A. Knight, C. M. Pueschel, Antifouling effects of epithallial shedding in three crustose coralline algae (Rhodophyta, Coralinales) on a coral reef. *J. Exp. Mar. Biol. Ecol.* **213**, 281–293 (1997).

36. R. S. Steneck, Escalating herbivory and resulting adaptive trends in calcareous algal crusts. *Paleobiology* **9**, 44–61 (1983).

37. J. Halfar, R. S. Steneck, M. Joachimski, A. Kronz, A. D. Wanamaker Jr., Coralline red algae as high-resolution climate recorders. *Geology* **36**, 463–466 (2008).

38. W. H. Adey, J. Halfar, B. Williams, The Coralline Genus *Clathromorphum* Foslie emend. Adey. *Smithson. Contrib. Mar. Sci.* **40**, 1–41 (2013).

39. B. B. Buchanan, W. Gruissem, R. L. Jones, *Biochemistry and Molecular Biology of Plants* (John Wiley & Sons, ed. 2, 2015).

40. M. A. Borowitzka, M. Vesk, Ultrastructure of the corallinaceae. I. The vegetative cells of *Corallina officinalis* and *C. cuvierii*. *Mar. Biol.* **46**, 295–304 (1978).

41. G. Flajs, Skeletal structures of some calcifying algae, in *Fossil Algae: Recent Results and Developments*, E. Flügel, Ed. (Springer Berlin Heidelberg, 1977), pp. 225–231.

42. M. S. Zamil, A. Geitmann, The middle lamella—More than a glue. *Phys. Biol.* **14**, 015004 (2017).

43. M. I. Bilan, A. I. Usov, Polysaccharides of calcareous algae and their effect on the calcification process. *Russ. J. Bioorganic Chem.* **27**, 2–16 (2001).

44. S. J. McCoy, C. A. Pfister, G. Olack, A. S. Colman, Diurnal and tidal patterns of carbon uptake and calcification in geniculate inter-tidal coralline algae. *Mar. Ecol.* **37**, 553–564 (2016).

45. P. T. Martone, D. A. Navarro, C. A. Stortz, J. M. Estevez, Differences in polysaccharide structure between calcified and uncalcified segments in the coralline *Calliarthron cheilosporioides* (Corallinales, Rhodophyta). *J. Phycol.* **46**, 507–515 (2010).

46. W. H. Adey, Y. M. Chamberlain, L. M. Irvine, An SEM-based analysis of the morphology, anatomy, and reproduction of *Lithothamnion tophiforme* (Esper) Unger (Corallinales, Rhodophyta), with a comparative study of associated north atlantic arctic/subarctic melobesioideae. *J. Phycol.* **41**, 1010–1024 (2005).

47. M. C. Nash, B. D. Russell, K. R. Dixon, M. Liu, H. Xu, Discovery of the mineral brucite (magnesium hydroxide) in the tropical calcifying alga *Polystrata dura* (Peyssonneliales, Rhodophyta). *J. Phycol.* **51**, 403–407 (2015).

48. F. Ragazzola, L. C. Foster, C. J. Jones, T. B. Scott, J. Fietzke, M. R. Kilburn, D. N. Schmidt, Impact of high CO_2 on the geochemistry of the coralline algae *Lithothamnion glaciale*. *Sci. Rep.* **6**, 20572 (2016).

49. A. Rösler, F. Perfectti, V. Peña, J. C. Braga, Phylogenetic relationships of Corallinaceae (Corallinales, Rhodophyta): Taxonomic implications for reef-building corallines. *J. Phycol.* **52**, 412–431 (2016).

50. D. L. Swofford, "PAUP*. Phylogenetic Analysis Using Parsimony (*and Other Methods). Version 4" (Sinauer Associates, 2002).

51. L. Bittner, C. E. Payri, G. W. Maneveldt, A. Couloux, C. Cruaud, B. Reviers, L. L. Gall, Evolutionary history of the Corallinales (Corallinophycidae, Rhodophyta) inferred from nuclear, plastidial and mitochondrial genomes. *Mol. Phylogenet. Evol.* **61**, 697–713 (2011).

52. A. Kato, M. Baba, S. Suda, Revision of the Mastophoroideae (Corallinales, Rhodophyta) and polyphyly in nongeniculate species widely distributed on Pacific coral reefs. *J. Phycol.* **47**, 662–672 (2011).

53. A. Caragnano, A. Foetisch, G. W. Maneveldt, L. Millet, L.-C. Liu, S.-M. Lin, G. Rodondi, C. E. Payri, Revision of Corallinaceae (Corallinales, Rhodophyta): Recognizing *Dawsoniolithon* gen. nov., *Parvicellularium* gen. nov. and Chamberlainoideae subfam. nov. containing *Chamberlainium* gen. nov. and *Pneophyllum*. *J. Phycol.* **54**, 391–409 (2018).

54. S. J. McCoy, N. A. Kamenos, Coralline algae (Rhodophyta) in a changing world: Integrating ecological, physiological, and geochemical responses to global change. *J. Phycol.* **51**, 6–24 (2015).

55. M. A. Borowitzka, Photosynthesis and calcification in the articulated coralline red algae *Amphiroa anceps* and *A. foliacea*. *Mar. Biol.* **62**, 17–23 (1981).

56. W. E. Piller, M. Rasser, Rhodolith formation induced by reef erosion in the Red Sea, Egypt. *Coral Reefs* **15**, 191–198 (1996).

57. A. B. Smith, A. Kroh, Phylogeny of Sea Urchins, in *Sea Urchins: Biology and Ecology*, J. M. Lawrence, Ed. (Elsevier, 2013), vol. 38, pp. 1–14.

58. M. Rasser, W. E. Piller, Depth distribution of calcareous encrusting associations in the northern Red Sea (Safaga, Egypt) and their geological implications, in *Proceedings of the 8th International Coral Reef Symposium* (1997), pp. 743–748.

59. C. H. C. Turner, L. V. Evans, Translocation of photoassimilated ^{14}C in the red alga *Polysiphonia lanosa*. *Br. Phycol. J.* **13**, 51–55 (1978).

60. Y. M. Chamberlain, Observations on the crustose coralline red alga *Spongites yendoi* (Foslie) comb. nov. in South Africa and its relationship to *S. decipiens* (Foslie) comb. nov. and *Lithophyllum natalense* Foslie. *Phycologia* **32**, 100–115 (1993).

61. T. Masaki, Studies on the Melobesioideae of Japan. *Mem. Fac. Fish. Hokkaido Univ.* **16**, 1–80 (1968).